Geophys. J. Int. (2002) **149,** 22–36

Ultrasonic velocity measurements in volcanic rocks: correlation with microtexture

T. Vanorio,[1] M. Prasad,[1] D. Patella[2] and A. Nur[1]

[1] *SRB Project, Geophysics Department, Stanford University, Stanford,* CA 94305, *USA. Email: tvanorio@stanford.edu, manika.prasad@stanford.edu, amos.nur@stanford.edu*

[2] *Department of Physical Sciences University Federico II, Naples, Italy. Email: patella@na.infn.it*

Accepted 2001 August 16. Received 2001 August 12; in original form 2000 August 30

SUMMARY

This paper summarizes results of a study of porosity, permeability, microstructure and acoustic properties of volcanic and pyroclastic rocks from Campi Flegrei (CF) and Mt. Etna (ET), Italy. We have measured the hydraulic, transport and acoustics properties of 28 room-dry samples at ambient conditions, 25 room-dry samples under confining pressure (up to 60 MPa) and 5 brine saturated samples under pressure (up to 45 MPa effective pressure). We established the following range of porosity, permeability, and V_p and V_s variations as functions of mineralogy and differential pressure in CF and ET lithologies:

1 Porosity
  CF pyroclastic rocks 30–60 per cent
  CF and ET lava rocks 2–20 per cent
2 Permeability
  CF pyroclastic rocks 10–1000 mD
  CF and ET lava rocks 0.01–100 mD
3 Velocity and Quality Factor
  CF pyroclastic rocks V_p 2–3 km s^{-1} V_s 1–2 km s^{-1} Q_p 5–80
  CF and ET lava rocks V_p 3.5–5.5 km s^{-1} V_s 2–3 km s^{-1} Q_p 10–115

Mineralogy and microstructure govern the acoustic and petrophysical properties of these rocks under pressure. In pyroclastic rocks, changes in acoustic response are directly related to presence of zeolites and pumice and their reactions with the pore fluid. In dry conditions, collapse of the internal texture of pumice leads to decreasing velocity with pressure. In saturated conditions, the water–zeolite interactions compete with effects due to collapsing internal textures and so velocity change with pressure is not as pronounced. The microstructural changes were confirmed by analyses of optical, hydraulic and transport properties after pressure: CT-scans show a macroscopically more compact structure; under optical microscopy, pumice and zeolitized pumice appear shredded. A significant reduction in porosity and permeability is measured after pressurization. In lava rock samples, acoustic velocities increase in function of pressure and the velocity–pressure relationships are characteristic of samples with rounded pores.

Our results emphasize the importance of conducting velocity measurements at simulated *in situ* conditions. By constraining the computations using site- and depth- specific rock physics properties, differences between ground deformation models in volcanic areas can be assessed and predicted more reliably thus reducing volcanic hazard.

Key words: caldera, earthquakes, igneous rocks, porosity, seismic velocities.

1 INTRODUCTION

The volcanic and seismic activity in the Mediterranean area is strongly linked to the geodynamic processes responsible for the formation of the Apennine Chain and the opening of the Tyrrhenian basin. Although the volcanic activities of Mt. Etna, Catania, Italy and the Campi Flegrei, Naples, Italy fit in this setting, they have distinctive features and local characteristics that make it difficult to assess their plate tectonics background.

The Campi Flegrei volcanic complex is an explosive caldera related to collapses accompanying the eruptions of the Campanian Ignimbrite (CI, 35–37 ka) (Rosi *et al.* 1983) and of the Neapolitan Yellow Tuff (NYT, 12 ka) (Lirer *et al.* 1987). Orsi *et al.* (1996) refers to it as a 'nested caldera structure'

resulting from both the aforementioned collapses. The recent bradyseismic crises in 1969–1971 and in 1982–1984, generating an uplift of 3.5 m around the town of Pozzuoli, attest to a still active magmatic system. The central part of this caldera is correlated with a gravity minimum, a zone of low seismic velocity and high V_p/V_s ratios (Cassano & La Torre 1986; Agip 1987). These data together with well data (Agip 1987; Carella & Guglielminetti 1983) have been interpreted as belonging to a low-density and highly fractured water saturated material extending up to 3 km depth (Ferrucci *et al.* 1992; Aster *et al.* 1990). The intense fluid circulation within the shallower zone and the pressure related to it might be responsible both for the ground deformation and seismicity (Casertano *et al.* 1976; Bonafede 1990) but the question about the triggering mechanism is still open.

Similarly, Mt. Etna volcano continuously shows signs of unrest characterized by volcanic eruptions and strong seismicity, mainly on the eastern flank. The volcanic activity has resulted from a mantle diapir emplaced about 500 ka, giving rise to a permanent deep reservoir (20–30 km) with tholeitic and alkali-basalt lavas and temporary shallow chambers with differentiated lavas (trachybasalt and trachyandesites) (Tanguy *et al.* 1997).

Renewal of volcanic and seismic activity at Campi Flegrei and at Mt. Etna always poses a serious hazard for these densely populated regions. For this reason, these areas are currently the targets of comprehensive research and surveillance programs. Geophysical and volcanological surveys have resulted in interpretative models that require knowledge about the subsurface (Loddo *et al.* 1989; Hirn *et al.* 1991; Di Maio & Patella 1994; Mauriello *et al.* 1997). Reliability of such models can be improved with *a priori* information about subsurface rock properties. Whereas the literature on *in situ* geophysical data is particularly prolific, laboratory measurements of rock physics properties under pressure are almost nonexistent for these areas (Zamora *et al.* 1994). Such measurements, however, will help us both to create reliable models, for example, of ground deformation at Campi Flegrei and to provide new tools that can be used for the prediction of the risk.

This study investigates the effects of lithology, microstructure, permeability, porosity and pressure on *P*- and *S*-wave velocity (V_p, V_s) and *P*-wave quality factor (Q_p) in about 30 ET and CF samples. The velocity measurements have been conducted under *in situ* conditions of pressure to simulate up to 3 km overburden (60 MPa).

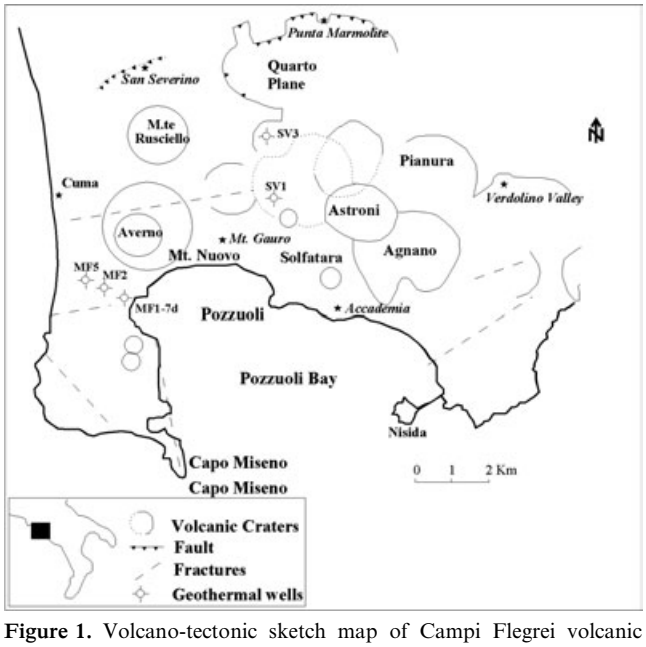

Figure 1. Volcano-tectonic sketch map of Campi Flegrei volcanic complex showing the location of geothermal wells. MF = Mofete well, SV = San Vito well, the samples locations are marked by stars.

Table 1. Lithology and samples location for CF.

Name	Lithol.	Sample Location	Name	Lithol.	Sample Location
SS	NYT	San Severino-Pozzuoli	**SN**	CI	S. Nicola la Str.– (*yellow facies*)
VR	NYT	Verdolino Valley-Naples	**VR_{CI}**	CI	Verdolino Valley (Piperno)
GA	NYT	Mount Gauro-Pozzuoli	**AC**	TRH	Pozzuoli- Accademia
SFF	CI	Furnolo- Caserta (*grey facies*)	**CU**	TRH	Cuma
SG1	CI	S. Agata dei Goti (*grey facies*)	**PM**	TRH	Punta Marmolite
SG2	CI	S. Agata dei Goti (*yellow facies*)			

Table 2. Lithology and samples location for ET.

Name	Lithol.	Sample Location	Name	Lithlol.	Sample Location
413	OLT	Aci Castello Complex (SE)	**1434**	PTB	Santa Tecla cliff (SE)
588	OLT	Adrano cliff (SW)	**1630**	PTB	Acireale Cliff (SE)
432	PGT	S. Maria di Licodia (SW)	**1132**	PTB	Tre Mestieri (SSE)
118	TRT	Neck of Motta di S. Anastasia (S)	**1049**	PTA	Simeto Valley (SW)
1612	TRT	Timpa S. Caterina at sea level (SE)	**1309**	ATT	Poggio la Naca (SSW flank)
1606	PAB	Timpa S. Caterina above 1612 (SE	**1678**	ABT	Mount Maletto (W)
623	PAB	Patenò Neck (SW)	**1824**	ABT	Mt. Spagnolo Erupt.
624	PAB	flow near Valcorrente (SSW)	**1810**	ABT	Mt. Spagnolo Erupt. (NW)
1603	PAB	flow from Contrada Malastalla			

2 METHODS AND MATERIAL

Volcanic rocks are the main lithologies in CF and ET areas. The different mineralogical composition reflects their diverse geodynamic environments. CF samples range from trachybasalt to peralkaline phonolitic trachytes; intermediate rocks are represented by latites, trachytes and alkali-trachytes (Armienti *et al.* 1983; Rosi & Sbrana 1987; Civetta *et al.* 1991). Lithology and location of the CF samples used in this study are shown in Table 1 and Fig. 1, respectively. Composition of ET samples (Table 2) ranges from tholeitic to alkaline series (see Fig. 2 for sample locations).

2.1 CF and ET sample lithology

Neapolitan Yellow Tuff (NYT), Campanian Ignimbrite (CI), and trachytic lava rocks (TRH) represent the main volcanic products in CF area. However, lava flows and domes are small

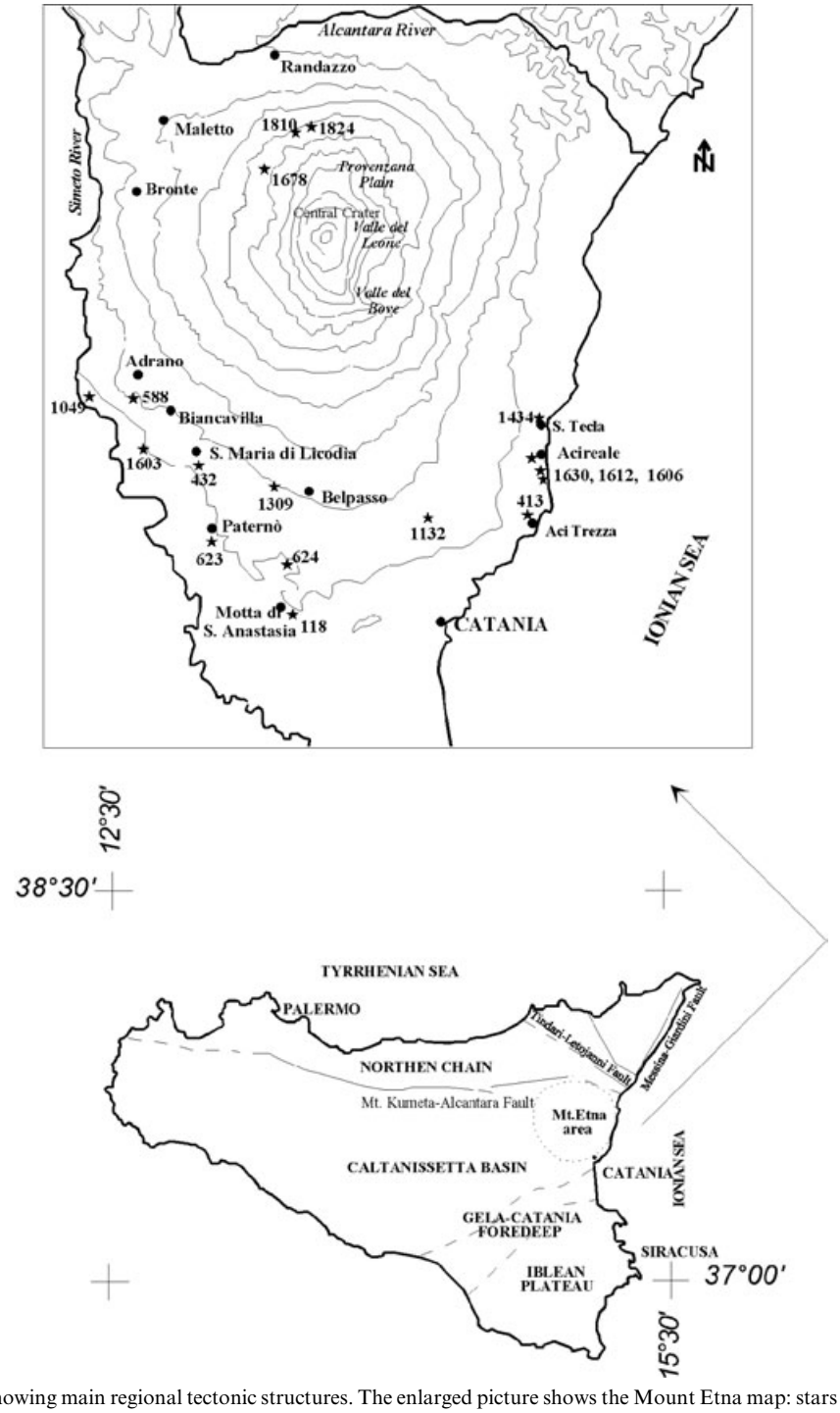

Figure 2. Map of Sicily showing main regional tectonic structures. The enlarged picture shows the Mount Etna map: stars mark the sample locations.

in volume and belong to the precaldera period. NYT is a highly inhomogeneous pyroclastic flow that has a vesicular feature containing unevenly distributed cavities, pumice and crystals of sanidine, pyroxene and biotite. CI is the largest pyroclastic deposit of the Campanian area (*c.* 30 000 km^2) ranging in composition from trachyte to phonolitic–trachyte (Civetta *et al.* 1997). It can be separated into a yellow (Campanian Ignimbrite Yellow Facies-CIYF) and a grey facies (Campanian Ignimbrite Gray Facies-CIGF). Almost all samples are free of macroscopic fracture; two of them (1824 and 1810) show big voids due to outgassing. In this study, samples of NYT, CI (CIYF and CIGF) and TRH have been selected from Campi Flegrei. Both, NYT and CIYF have experienced intense zeolitization. Sersale (1958) has shown that pozzolana, a glassy trachytic product, changes to tuff after cementation due to zeolitization. Powder X-ray diffraction analysis shown that the yellowish, nearly isotropic matrix, consists mostly of chabazites and phyllipsite (Lenzi & Pozzuoli 1970). CIYF, consists mainly of chabazite ($\approx$70 per cent) with about 10 per cent of phillipsite whereas NYT contains predominantly (up to about 80 per cent) phillipsite.

For this study, Olivine–Tholeite samples (OLT), Pigeonite Tholeites (PGT), Transitional Tholeites (TRT), Porphyritic Alkali Basalt (PAB), Porphyritic Trachybasalt (PTB), Porphyritic Trachyandesite (PTA), Aphanitic Trachyandesite (ATT) and Aphyric Basalt (ABT) were selected from ET area. XRF mineralogical composition was available for each sample (Tanguy *et al.* 1997).

2.2 Sample preparation

Particular attention was dedicated to the collection procedure to avoid sampling in altered layers. Cylindrical core samples of 2.5 cm diameter and 3.0 cm length, with their faces parallel to within 0.1 mm were prepared from each sample. These samples were used for porosity, permeability, CT-scans, and ultrasonic measurements.

2.3 Experimental procedures

He-porosity ($\pm$1 per cent), bulk and grain densities ($\pm$1 per cent) and Klinkenberg-corrected air permeability ($\pm$2 per cent) were measured in all samples at room *PT* conditions. Microstructure was studied with optical microscopy of thin sections prepared from faces cut parallel to the length of the samples. Blue dye epoxy was used to enhance pore space recognition. CT scans were used to map larger scale density variations in the samples. CT scan was performed with a 3-mm scan width and a step of 2 mm. To understand effects of pressure, these analyses were made on the NYT samples before and after pressure tests.

The pulse transmission technique (Birch 1960) was used for V_p and V_s measurements. *P*-wave quality factor (Q_p) was

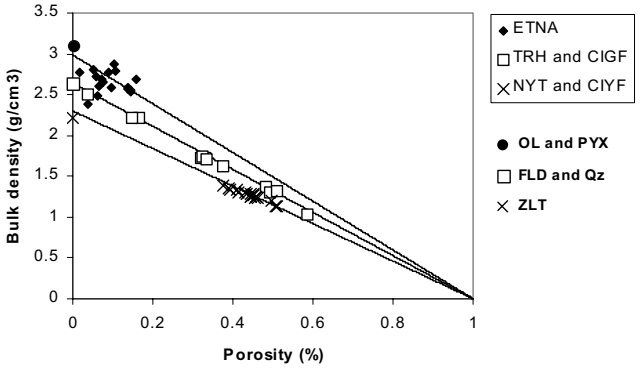

Figure 3. Porosity-bulk density relationship for CF and ET samples. At 0 per cent of porosity the grain densities of minerals forming rocks are reported. Error on porosity is 0.01 per cent; the error bar in porosity is smaller than the size of plotted symbols.

Table 3. Summary of physical property data for CF and ET samples

Lithology	Sample	Porosity (%)	Permeability (mD)	Grain density (g cm^{-3})	Bulk density (g cm^{-3})
CF SAMPLES					
NYT	GA_3	37.68	15.3	2.23	1.39
	GA_2	38.99	69.4	2.23	1.36
	GA_1	39.24	18.0	2.27	1.38
	VR_4	40.90	25.6	2.26	1.34
	VR_3	41.39	18.9	2.23	1.31
	VR_1	43.08	Na*	2.29	1.30
	VR_2	44.49	27.7	2.25	1.25
	SS_2	45.10	87.9	2.30	1.26
	SS_1	45.91	Na	2.32	1.25
	SS_3	46.23	134.0	2.29	1.23
CIYF	SG2_4	43.48	32.3	2.28	1.29
	SG2_3	44.8	117.9	2.26	1.26
	SG2_1	44.6	Na	2.31	1.28
	SN_2	45.30	8.9	2.35	1.28
	SG2_2	45.69	23.2	2.28	1.24
	SN_1	49.72	Na	2.38	1.20
	SN_3	50.54	16.5	2.31	1.14
	SN_4	50.89	54.6	2.30	1.13
CIGF	SFF_2	32.22	35.2	2.54	1.72
	SFF_3	32.48	41.2	2.57	1.74
	SFF_1	33.21	42.6	2.57	1.72
	SFF_4	33.42	49.5	2.57	1.71
	VRci_4	37.66	>1000	2.61	1.63
	VRci_1	48.31	>1000	2.64	1.37
	VRci_2	49.38	>1000	2.56	1.30
	VRci_3	50.99	>1000	2.70	1.32
	SG1_1	58.49	Na	2.50	1.04
TRH	CU	3.82	<0.01	2.60	2.50
	PM	14.95	<0.01	2.60	2.22
	AC	16.72	5.2	2.65	2.21
ET SAMPLES					
OLT	413	6.36	1.9	2.66	2.49
	588	13.71	<0.0	3.00	2.59
PGT	432	13.71	92.8	2.98	2.57
TRT	118	1.86	<0.01	2.83	2.75
	1612	6.57	<0.01	2.79	2.60
PAB	1606	3.91	<0.01	2.99	2.88
	1603	5.05	<0.01	2.95	2.80
	623	10.42	<0.01	3.00	2.69
	624	15.99	<0.01	2.83	2.38
PTB	1434	7.14	8.8	2.90	2.69
	1132	7.69	<0.01	2.87	2.65
	1630	10.65	<0.01	3.12	2.79
PTA	1049	5.91	<0.01	2.90	2.72
ATT	1309	9.62	1.6	2.86	2.59
ABT	1678	9.07	<0.01	3.05	2.77
	1824	14.44	2.1	2.96	2.53
	1810	14.59	1.7	2.98	2.55

calculated, where signal quality allowed it, from the stored signal waveforms using the spectrum division technique (Toksöz *et al.* 1979; Prasad & Manghnani 1997). In order to ensure similar coupling and pressure conditions both for the sample and reference, the signal from an aluminium cylinder of the same size was recorded at various pressure steps and used as reference signal at that pressure. Note, that the reported Q_p values are apparent Q: they represent the combined effects of scattering and intrinsic attenuation.

The bench-top acoustic setup consisted of a digital oscilloscope (Tektronix TDS 420 A), a pulse generator (Panametrics 5052 PR) and two pairs of transducers (Panametrics V103 for 1 MHz *P*-waves and V154 for 0.7 MHz *S*-waves).

The experimental setup for the pressure tests (Prasad *et al.* 1999; Prasad & Nur 2002) consisted of a digital oscilloscope (Tektronix TDS 420 A) and a pulse generator (Velonex 345). The sample was jacketed with rubber tubing to isolate it from the confining pressure medium. PZT-crystals mounted on steel endplates were used to generate *P*- and *S*-waves. The principal frequency was about 1 MHz for *P* and 700 MHz for *S*-waves. A high viscosity bonding medium (Panamterics SWC) was used to bond the endplates to the sample. A pore fluid inlet in each endplate allowed passage of pore fluids through the sample. Three linear potentiometers were used to measure length changes of the samples as a function of stress. The length change was directly related to changes in porosity by assuming that pore collapse was the main cause of strain. The experimental configuration allowed simultaneous measurements of *P*- and *S*-waves at various confining pressures up to 60 MPa. In this paper, only results of V_p, V_s, and Q_p will be discussed. A complete description of the experimental set-up used in this study can be found in Prasad *et al.* (1999) and Prasad & Nur (2002).

Traveltime was measured after digitizing each trace with 1024 points at a time sweep of 5 μs, thus allowing a time resolution of about 5 ns or about 0.2 per cent error in velocity. Actual error in velocity measurement is estimated to be around 1 per cent due to operator error in picking first arrival. The system delay time was measured by taking head-to-head time at 2 MPa. The travel-time calibration was confirmed by measuring an aluminium cylinder at different pressures.

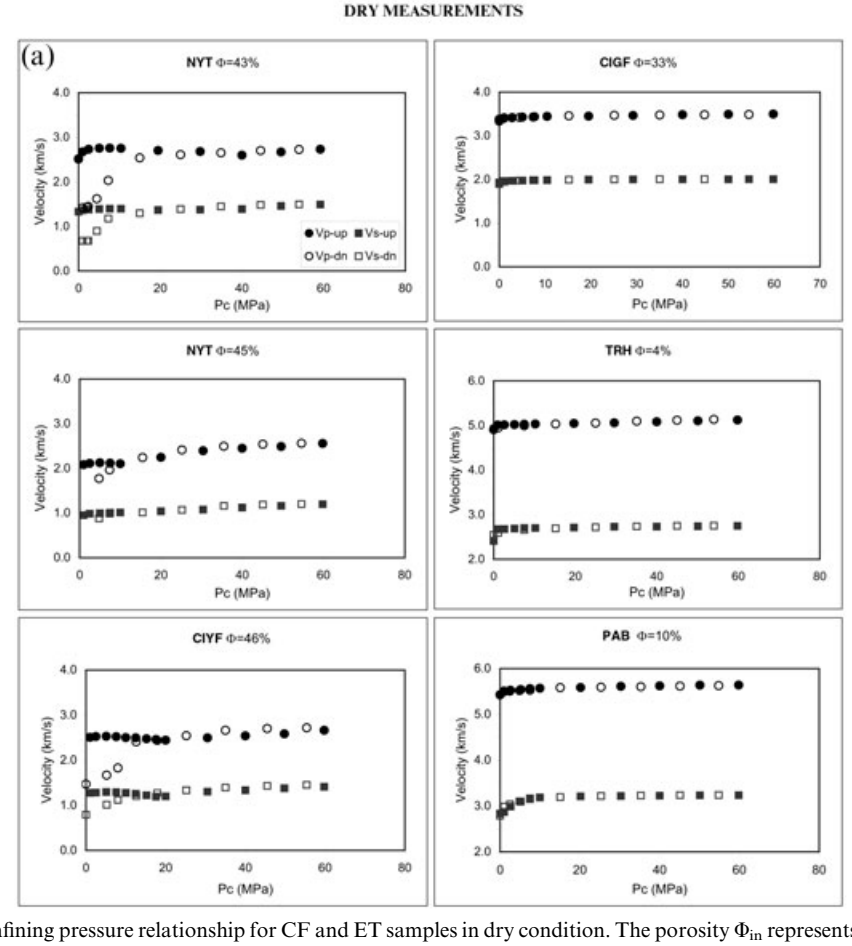

Figure 4. (a) Velocity-confining pressure relationship for CF and ET samples in dry condition. The porosity Φ_{in} represents the initial sample porosity. Close circles are used for up pressure cycle, open circles for the down cycle. Error on velocity is 1 per cent; the error bar in the velocity plots is smaller than the size of used symbols. (b) Velocity, V_p/V_s, Elastic moduli, Porosity, Poisson's ratio and Quality factor versus confining pressure for a CIYF dry sample. The porosity Φ_{in} represents the initial sample porosity. Close circles are used for up pressure cycle, open circles for the down cycle. Error on velocity is 1 per cent; the error bar in the velocity plots is smaller than the size of used symbols. (c) Velocity, V_p/V_s, Elastic moduli, Porosity, Poisson's ratio and Quality factor versus confining pressure for a NYT dry sample. The porosity Φ_{in} represents the initial sample porosity. Close circles are used for up pressure cycle, open circles for the down cycle. Error on velocity is 1 per cent; the error bar in the velocity plots is smaller than the size of used symbols. (d) Velocity, V_p/V_s, Elastic moduli, Porosity, Poisson's ratio and Quality factor versus confining pressure for a CIGF dry sample. The porosity Φ_{in} represents the initial sample porosity. Close circles are used for up pressure cycle, open circles for the down cycle. Error on velocity is 1 per cent; the error bar in the velocity plots is smaller than the size of used symbols.

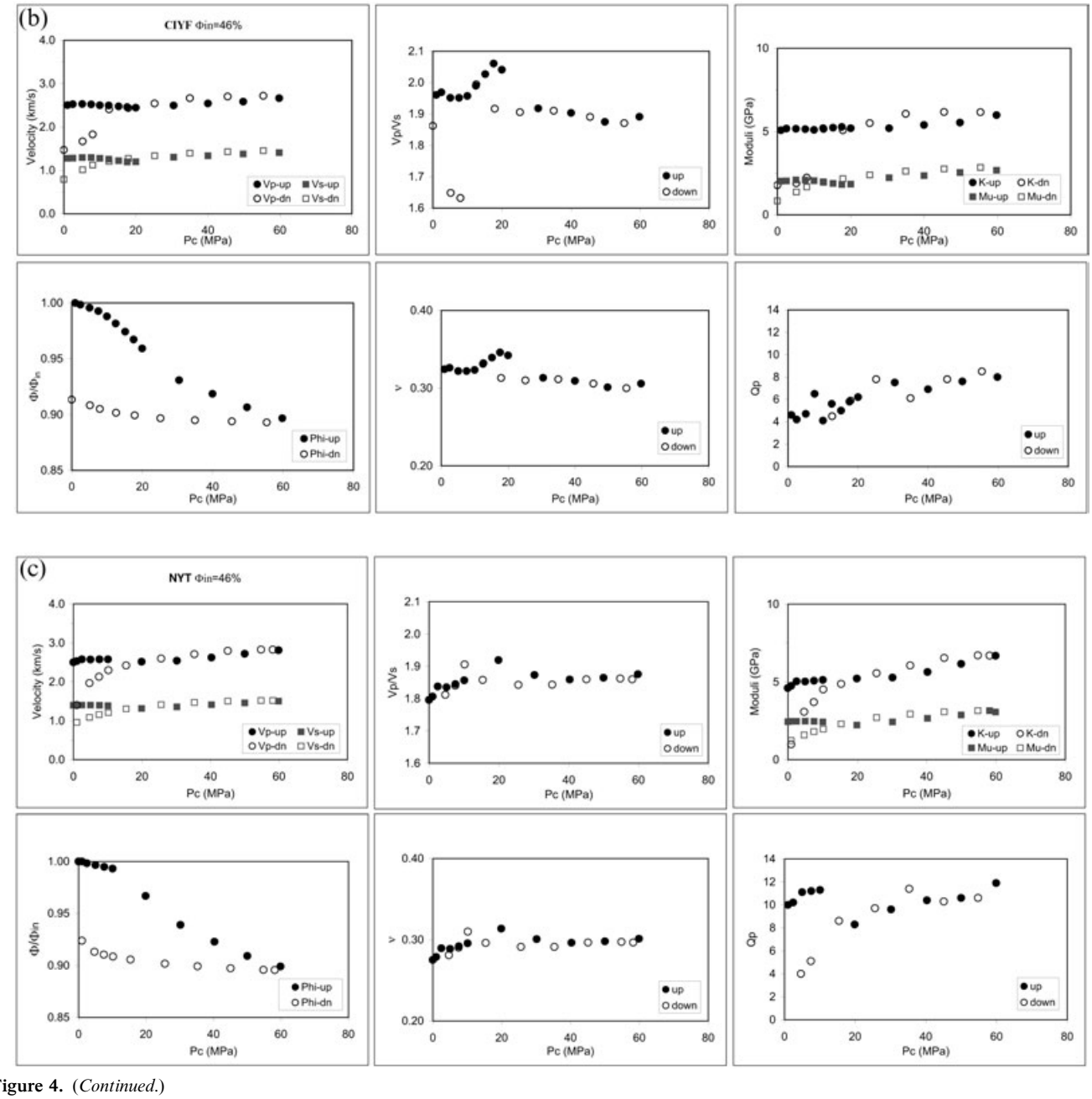

Figure 4. (*Continued.*)

3 RESULTS

3.1 Porosity and permeability

Porosity and permeability values of all samples are given in Table 3. Tuffs and ignimbrites showed a porosity range of 30–60 per cent and a permeability range between 10 mD–140 mD; for trachytic lavas (THR), the porosity range between 2 and 20 per cent and the permeability was <5 mD. The ET samples show a lower porosity 2–16 per cent and permeability <9 mD. The porosity range for tuff and ignimbrite samples is comparable with the porosity measurements carried out with the grain density method on the same kind of samples (Vanorio 1998) so, it is plausible that their pores are completely interconnected. In thin section, these samples showed a very porous frame due to the zeolitized matrix and the pumice structure. Fig. 3 shows the porosity-bulk density relationship. It is easy to see three trends: (1) the zeolitized facies NYT and CIYF; (2) TRH and CIGF that have same trachytic composition; (3) ET group, here it is not possible to distinguish between the different mineralogy of the samples. Solid lines describe the theoretical porosity–density pattern given by the following formula:

Grain density (ρ_g) used in the formula was calculated from the grain densities of the mineral composition of the rocks taken from Tanguy *et al.* (1997) and Rosi & Sbrana (1987). We used air density as fluid density (ρ_{fl}) since samples were oven dried.

In Fig. 3, the zero porosity points indicate grain densities of the main minerals forming the samples used in this study (Carmichael 1989).

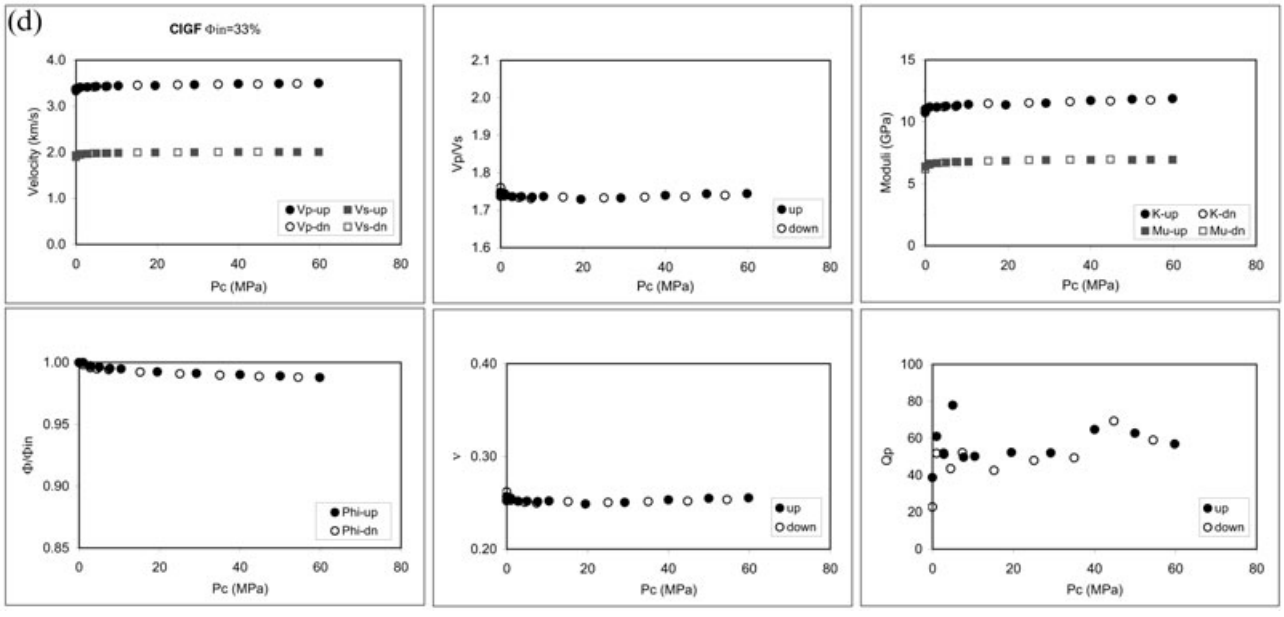

Figure 4. (*Continued.*)

In addition to porosity, bulk density is also controlled by mineralogy. The ET basalt samples mainly follow the trend of the alkaline basalts enriched in olivine and pyroxenes. Whereas ET samples with a higher silica and feldspars content (i.e. tholeitic basalts) (Tanguy *et al*. 1997) departure from this trend. Trachytic ignimbrites and lava samples fall on another trendline since they are mainly enriched in quartz and feldspars. Zeolitized tuffs and ignimbrites make up the third group with the lowest bulk density. Their end points crossplot with grain density for chabazite and phillipsite.

Table 4. Summary of acoustic property data for CF and ET samples

Sample	Pressure =0 Mpa		Pressure =5 Mpa		Pressure =10 Mpa		Pressure =20 Mpa		Pressure =30 Mpa		Pressure =40 Mpa		Pressure =50 Mpa		Pressure =60 Mpa	
	V_p (Km/s)	V_s	V_p (Km/s)	V_s	V_p (Km/s)	V_s	V_p (Km/s)	V_s	V_p (Km/s)	V_s	V_p (Km/s)	V_s	V_p (Km/s)	V_s	V_p (Km/s)	V_s
GA_2	2.60	1.20	2.62	1.21	2.64	1.22	2.62	1.21	2.60	1.19	2.56	1.17	2.56	1.17	2.60	1.18
GA_1	2.72	1.44	2.80	1.61	2.80	1.61	2.82	1.61	2.78	1.58	2.74	1.54	2.73	1.54	2.75	1.55
VR_1	2.52	1.33	2.76	1.39	2.75	1.40	2.71	1.37	2.68	1.38	2.60	1.39	2.67	1.46	2.73	1.49
VR_2	2.50		2.52	1.00	2.58	1.01	2.57	1.04	2.51	1.07	2.48	1.10	2.54	1.13	2.57	1.16
SS_2	2.08	0.95	2.13	0.99	2.10	1.01	2.25	1.04	2.39	1.08	2.45	1.12	2.49	1.16	2.56	1.20
SS_1	2.50	1.39	2.57	1.40	2.57	1.39	2.52	1.31	2.54	1.36	2.62	1.41	2.72	1.46	2.81	1.50
SG2_3	3.62	1.24	3.55	1.28	3.54	1.27	3.50	1.21	3.45	1.25	3.48	1.29	3.52	1.31	3.53	1.34
SG2_2	2.51	1.28	2.53	1.30	2.50	1.28	2.45	1.20	2.50	1.30	2.54	1.34	2.59	1.38	2.66	1.41
SN_1	2.52	1.18	2.64	1.04	2.60	1.03	2.58	1.04	2.62	0.97	2.65	0.88	2.74		2.77	
SFF_1	3.37	1.93	3.43	1.97	3.44	1.98	3.45	1.99	3.46	2.00	3.48	2.00	3.49	2.00	3.50	2.00
CU	4.91	2.41	5.02	2.69	5.03	2.70	5.05	2.71	5.06	2.73	5.08	2.73	5.10	2.74	5.12	2.75
PM	4.49	2.50	4.55	2.57	4.56	2.59	4.60	2.60	4.62	2.62	4.63	2.62	4.68	2.64	4.68	2.64
AC	3.42	1.80	3.71	1.93	3.79	2.00	3.95	2.08	4.07	2.15	4.15	2.20	4.21	2.24	4.35	2.29
413	4.54	2.58	4.58	2.62	4.60	2.64	4.62	2.66	4.63	2.66	4.67	2.67	4.67	2.68	4.69	2.68
432	5.03	2.85	5.11	2.95	5.12	2.96	5.16	2.98	5.24	3.00	5.28	3.02	5.37	3.05	5.42	3.07
118	5.34	3.01	5.44	3.14	5.45	3.15	5.46	3.15	5.46	3.16	5.47	3.16	5.47	3.16	5.48	3.16
1612	5.44	2.96	5.49	3.01	5.51	3.02	5.52	3.03	5.53	3.03	5.55	3.04	5.55	3.04	5.59	3.06
623	5.43	2.84	5.54	3.09	5.57	3.19	5.59	3.21	5.61	3.22	5.62	3.23	5.64	3.23	5.64	3.24
624	4.60	2.32	4.70	2.38	4.72	2.40	4.73	2.42	4.77	2.44	4.82	2.45	4.87	2.47	4.90	2.48
1434	5.64	2.97	5.85	3.06	5.87	3.13	5.89	3.24	5.93	3.26	5.96	3.27	5.95	3.28	5.97	3.29
1630	5.68	2.84	5.80	3.23	5.82	3.25	5.84	3.26	5.84	3.26	5.86	3.27	5.90	3.28	5.93	3.29
1309	4.64	2.57	4.78	2.68	4.82	2.71	4.93	2.78	5.05	2.84	5.15	2.90	5.25	2.94	5.32	2.97
1678	5.08	2.75	5.17	3.08	5.19	3.09	5.23	3.10	5.28	3.10	5.34	3.12	5.40	3.13	5.44	3.16
1824	4.15	2.42	4.36	2.56	4.42	2.61	4.63	2.69	4.84	2.77	5.03	2.85	5.20	2.90	5.35	2.95
1810	3.88	2.29	4.07	2.39	4.19	2.46	4.51	2.57	4.70	2.66	4.95	2.76	5.10	2.86	5.23	2.93

3.2 Ultrasonic measurements

The following ultrasonic measurements have been performed:

V_p and V_s in room-dry CF and ET sample at ambient conditions (note: in subsequent text we shall refer to room-dry as dry)

Vp and V_s under varying confining pressure in dry CF and ET sample ($Pc_{max} = 60$ MPa). These conditions of pressure simulate up to 3 km overburden.

Vp and V_s under varying effective pressure (P_e) in selected saturated samples from CF and ET ($Pf_{max} = 15$ MPa, $Pe_{max} = 45$ MPa);

P-wave quality factor (Q_p)

3.2.1 Dry Measurements

A summary of V_p and V_s measurements as a function of pressure in the dry samples is given in Table 4. Fig. 4(a) shows typical examples of pressure effects on velocity for dry NYT, CIYF, CIGF, and TRH samples. All zeolitized samples containing pumice (NYT and CIYF) show a remarkable behaviour with increasing pressure. During the up-going pressure cycle, velocity first decreases with increasing pressure up to about 20 MPa. Between 20 MPa and 60 MPa velocity increases slightly with pressure, this change is reversible. Below 20 MPa, the velocity is much lower (for example, V_p can be 1 km s^{-1} lower) than the initial velocity. The CIGF, TRH, and ET samples do not show this behaviour. To emphasize the changes with pressure, we present details of typical CIYF (Fig. 4b) and NYT (Fig. 4c) samples. Figs 4(b,c) present variation of velocity, V_p/V_s, elastic moduli, change in porosity (Φ) normalized by initial porosity (Φ_{in}), Poisson's coefficient and P-wave quality factor versus pressure for NYT and CIYF, respectively. For comparison, Fig. 4(d) shows the same properties for a typical CIGF sample. In the CIYF and NYT samples, in addition to velocity changes, we observe:

A large irreversible change in porosity (calculated from length change, DL) with increasing pressure (up to 10 per cent). This change is much larger than that observed in sedimentary rocks of similar porosity (up to 2 per cent change (Prasad *et al.* 1999)).

The porosity change is not a continuous trend during the up cycle pressure: rate of change is low up to 15–20 MPa, it increases between 20 and 40 MPa, and, finally beyond 40 MPa, it is lower again. The decrease in length (i.e. porosity) is not reversible.

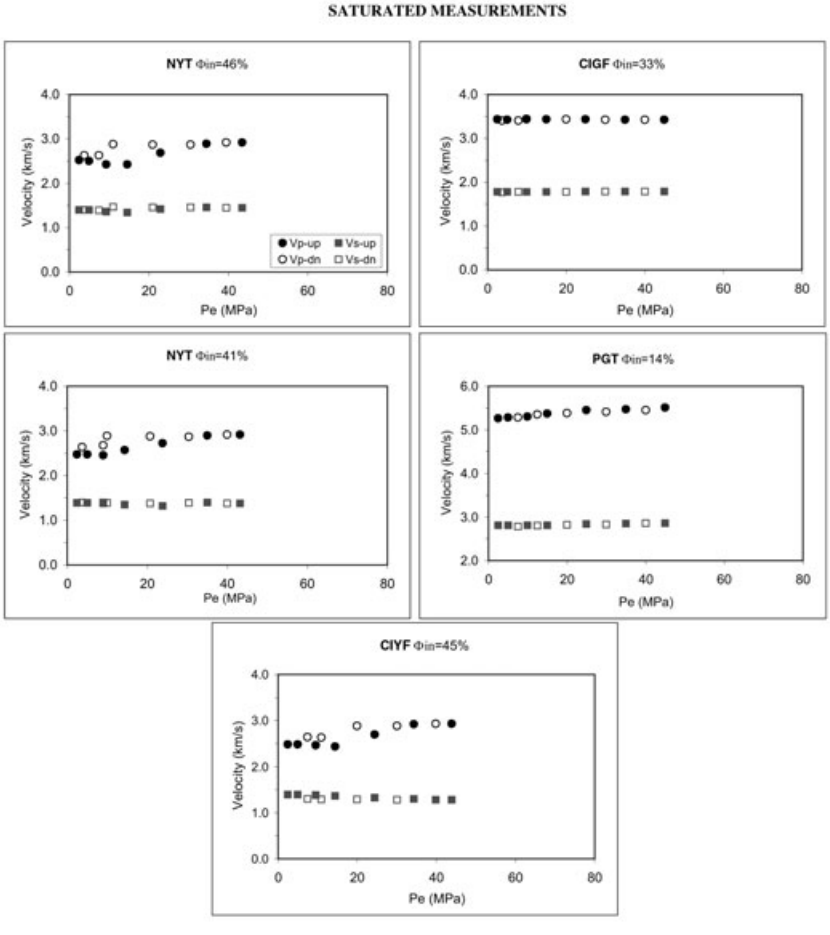

Figure 5. Velocity-effective pressure relationship for CF and ET samples in saturated condition. The porosity Φ_{in} represents the initial sample porosity. Close circles are used for up pressure cycle, open circles for the down cycle. Error on velocity is 1 per cent; the error bar in the velocity plots is smaller than the size of used symbols.

The V_p/V_s ratio versus pressure shows a maximum at 20 MPa implying that V_s, is more affected by the breaking of bonds than V_p. We postulate that the breaking of bonds compromises shear strength significantly.

Because of the closer step of velocity measurements, the minimum velocity at 20 MPa is much better defined for the CIYF sample (Fig. 4b) than NYT samples. Nevertheless further acoustic measurements versus pressure on pumice with 38 per cent porosity showed that velocity decreased with pressure up to 15–20 MPa, after 20 MPa, as the sample starts to compact, velocity increases slightly. On exhumation after the pressure cycle, the initially consolidated sample was found to have disintegrated.

In welded ignimbrite grey facies (CIGF) and lava samples (TRH and ET) velocity increases only slightly with pressure and both samples show a low pressure sensitivity (Fig. 4a,d). This implies a stiffer frame and rounded pores. In fact, in a pressure–velocity relationship, the amount of velocity change with pressure is directly depending on the amount of soft or crack-like pore space. Low aspect ratios also affect the range of

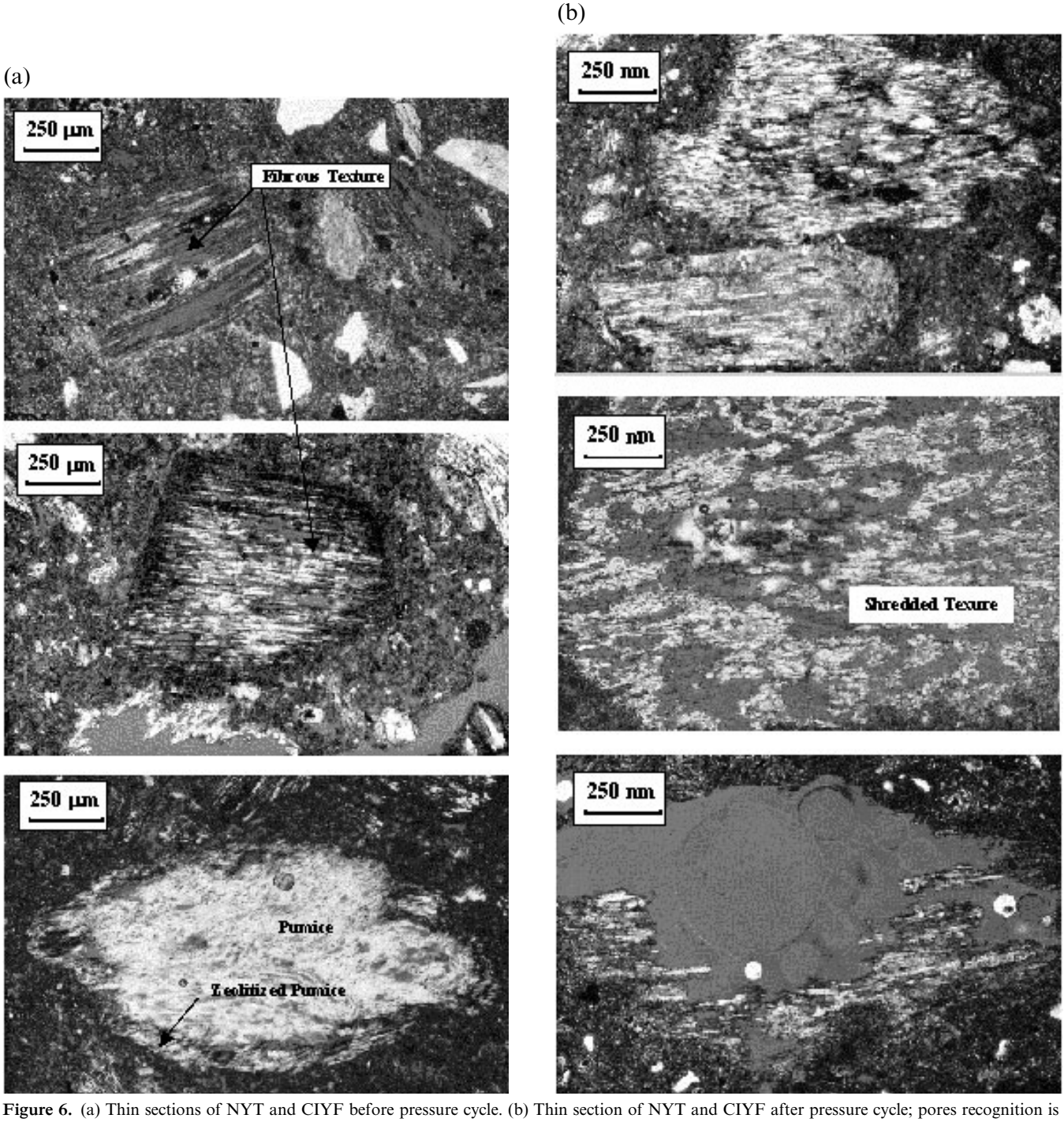

Figure 6. (a) Thin sections of NYT and CIYF before pressure cycle. (b) Thin section of NYT and CIYF after pressure cycle; pores recognition is enhanced by blue dye epoxy which appears as the grey colour in the figure. Cracks are visible around and within the pumice structure

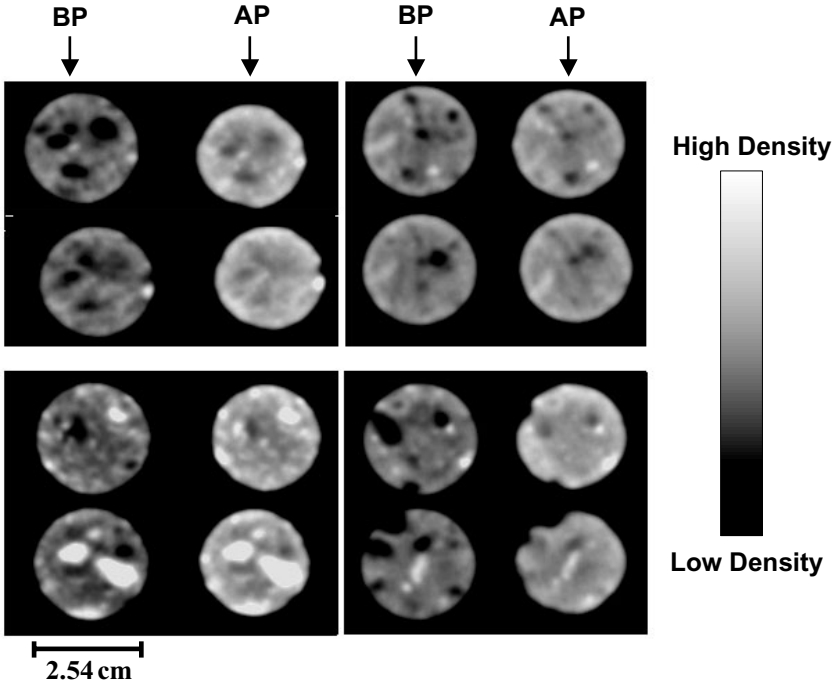

Figure 7. CT-scans on NYT and CIYF samples before (BP) and after (AP) pressurization.

the greatest pressure sensitivity. Rounded pores rather than crack-closure control, beyond 20 MPa, the velocity-pressure relationship in pyroclastic rocks (NYT and CIYF) as well.

3.2.2 Saturated Measurements

Five samples were saturated with brine and measured under pressure. Pore fluid pressure (Pf) was varied up to 15 MPa to permit a maximum effective pressure of 45 MPa. Fig. 5 shows the effects of effective pressure on velocity, for saturate NYT, CIYF and CIGF samples. Due to the difficulties in saturating the low permeability Etnean samples, only one sample (PGT) from this set was measured at pressure. The brine used to saturate samples reflects the chemical composition of fluids in Mofete well (Agip 1987). At this location, the system fluid /rock is in equilibrium condition and its composition is chlorine-alkaline type. Again, the zeolitized facies (NYT and CIYF) show a remarkable behaviour. After a small decrease in velocity with pressure up to 15–20 MPa, velocities strongly increase with pressure. When the pressure is released a hysteresis can be noted. The saturated CIGF samples so not show this behaviour.

4 SUMMARY OF RESULTS

Data collected in this work allows subdivision of the rocks based on their pressure trends: lavas and welded ignimbrite without zeolites and zeolitized tuff and ignimbrite. Main characteristics of these two trends are:

Lavas and welded ignimbrites without pumice and zeolites (ET, THR and CIGF):

higher grain density (>2.60 g cm-3),

dry and saturated measurements show similar characteristics,

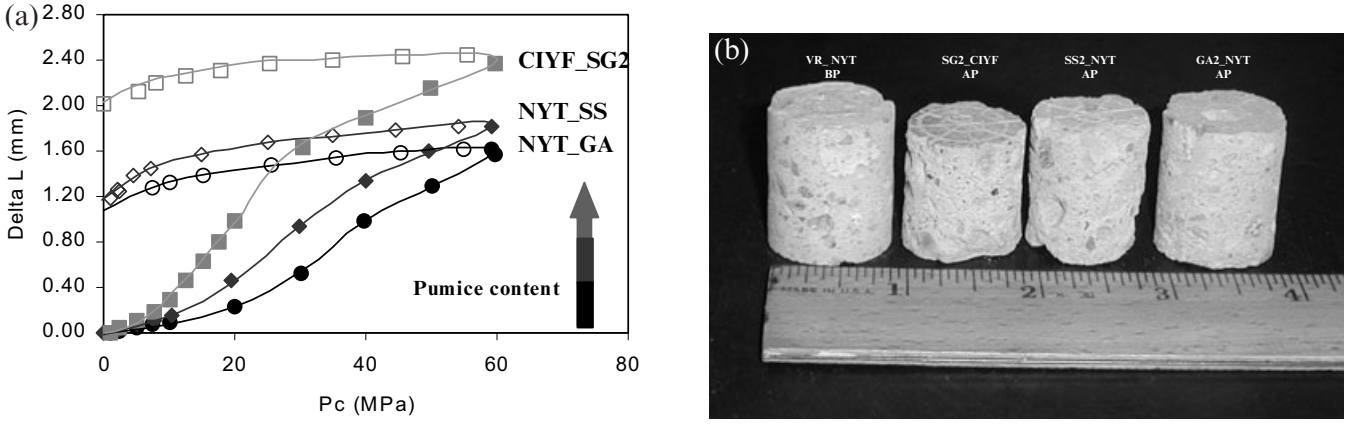

Figure 8. (a). Dependence of DL change rate on pumice content for NYT and CIYF samples. Three samples have different porosity: 39 per cent (GA_NYT, circles), 43 per cent (SS_NYT, diamonds) 46 per cent (SG2°CIYF, squares). (b) CF samples before (VR_NYT) and after pressurization (GA_NYT, SG2°CIYF and SS_NYT). Voids in the samples after pressurization have been formed by collapse of pumice.

small increase in velocity with increasing of P_e,
negligible change in DL with P_e,
quality factor ranges from 10 to 100
no porosity, permeability, and velocity hysteresis after pressure cycles,

Zeolitized Tuff and Ignimbrite (NYT and CIYF):

lower grain density ($\approx$2.2–2.3 g cm^{-3})

Up to 20 MPa

Dry samples: slight decrease in velocity up to 15–20 MPa; considerable decrease from the initial values during down cycle.
Saturated samples: slight decrease in velocity up to 15–20 Mpa.

Beyond 20 MPa

Dry samples: after 15–20 MPa velocity increases slightly
Saturated samples: after 15–20 MPa velocity increases considerably; negligible velocity hysteresis during down cycle
Quality factor values range from 4 to 12 almost independent of pressure
Significant length change with pressure, considerable hysteresis in dry samples

5 DISCUSSION

Our results show that zeolites and pumice significantly change the acoustic response. The following changes are observed in microstructure after pressure:

CT-scans show a macroscopically more compact structure.
Under optical microscopy pumice and zeolites appear shredded.
Porosity and permeability are reduced after pressurization.

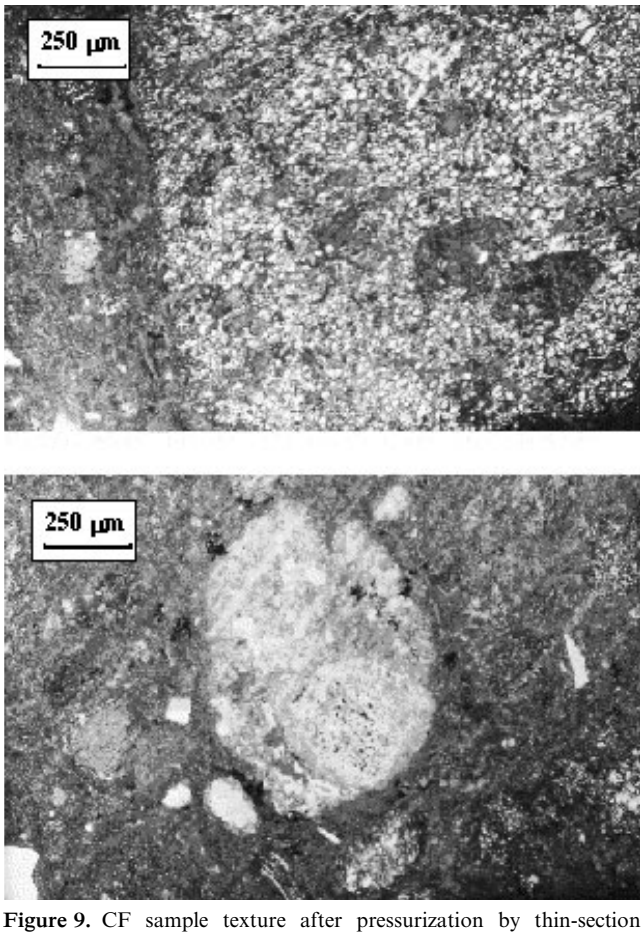

Figure 9. CF sample texture after pressurization by thin-section analysis. Cracks are visible around and within the zeolitized pumice structure.

5.1 Microstructure

Several thin sections of NYT and CIYF are shown in Figs 6(a,b). A comparison of the images before (Fig. 6a) and after the pressure cycle (Fig. 6b) shows that:

(1) The background matrix is very porous (grey colour = pore space). It consists mainly of zeolitized zones that show the characteristic fibrous structure. Pumice, plagioclase and occasionally sanidine crystals are randomly distributed in the matrix.

(2) The typical fibrous texture is completely shredded after the pressure cycle. Collapse of pumice texture and bond breaking around crystal and pumice are observed.

Although, for obvious reasons, thin-sections are not from the same position, this behaviour is observed in all thin-sections of NYT and CIYF.

In Fig. 7 textural variations mapped by CT-scans are showed for tuff and ignimbrite samples; macroscopic strains due to pressure cycle (i.e. length and diameter shortening) are clearly mapped as density variations. Samples after pressurization show a more dense and compact structure. At times, a reduction of less dense zones (pores or pumice) can also be observed.

Therefore, after pressurization, these samples showed a more compact structure at macroscopic scale and a shredded and cracked texture at the microscopic scale.

Fig. 8(a) shows that the DL change rate in samples with varying pumice content. Visual examination of the exhumed samples showed that the changes in length and V_p/V_s are lower in samples with smaller pumice content (e.g. Gauro's Tuff NYT_GA, Figs 8a,b). Since distinct V_p and V_s versus pressure trends have been noted in zeolitized facies containing pumice, we suggest that the acoustical and physical behaviour in dry condition are controlled by changes in the pumice (Figs 7 and 8), whereas water–zeolite interactions control them in the saturated case. Zeolites, in fact, are aluminosilicate minerals with and open framework of $[SiO_4]^{4-}$ and $[AlO_4]^{5-}$ polyhedra. They contain channels and cavities housing cations and water molecules. Their main properties can be summarized (Breck 1974; Dyer 1988; Gillet *et al.* 1996) as:

(1) Ion exchange—the cations have a high degree of mobility that facilitates ion exchange. Zeolites readily lose water molecules (intumescence) when heated and regain them at room condition (the word 'zeolite' has Greek roots and means boiling stones);

(2) Molecular sieving—the $[SiO_4]^{4-}$ and $[AlO_4]^{5-}$ tetrahedra create a porous structure in zeolites. They are arranged to form a regular array of apertures. These apertures act as sieves by selectively incorporating some molecules into their porous structure while rejecting others based on their effective molecular dimensions (Breck 1974; Dyer 1988)

(3) Adsorption—the adsorption of polar molecules on crystalline zeolites (host) is characterized by Langmuir-type isotherm, where the quantity adsorbed, relative to the quantity of complete pore-filling, is maximized already at very low

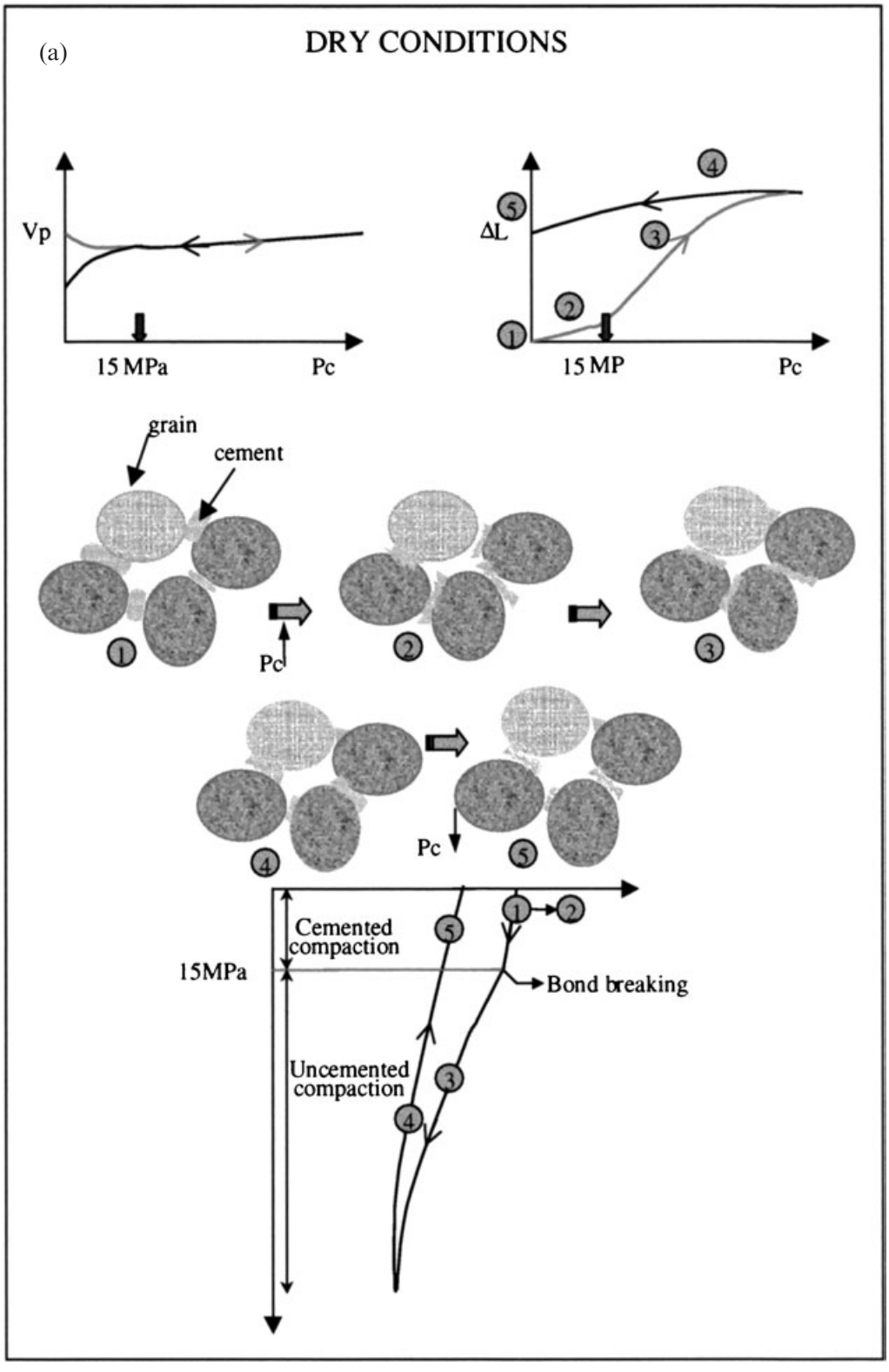

Figure 10. (a). Schematic diagram summarizing main steps of the hypothesis explained in the text, for dry conditions: Step 1: original sample. Step 2: increasing pressure leads to breaking bonds around crystals and pumice collapse; sample follows cemented compaction trend. Step 3: After 15–20 MPa, compaction become significant and follows the uncemented trend, breakdown of fibrous pumice structure. Step 4: On pressure release, velocity values follow uncemented compaction trend. Especially below 15–20 MPa, since the broken bonds cannot be mended, a strong velocity decrease is observed. (b) Schematic diagram summarizing main steps of the hypothesis explained in the text for saturated conditions. Step 1: original sample. Step 2: initial low rates of change associated with the bond-breaking and pumice collapse phase. Step 3: subsequent pressure increase leads to maximum compaction, marked velocity increase due to high absorption power of zeolites. Step 4: upon pressure release, trapped pore water due to pore collapse and to the aforementioned properties of zeolites lead to local pressure anomalies. These localized pore pressure changes might cause stiffening of the frame, leading to increase V_p; V_s would not be affected.

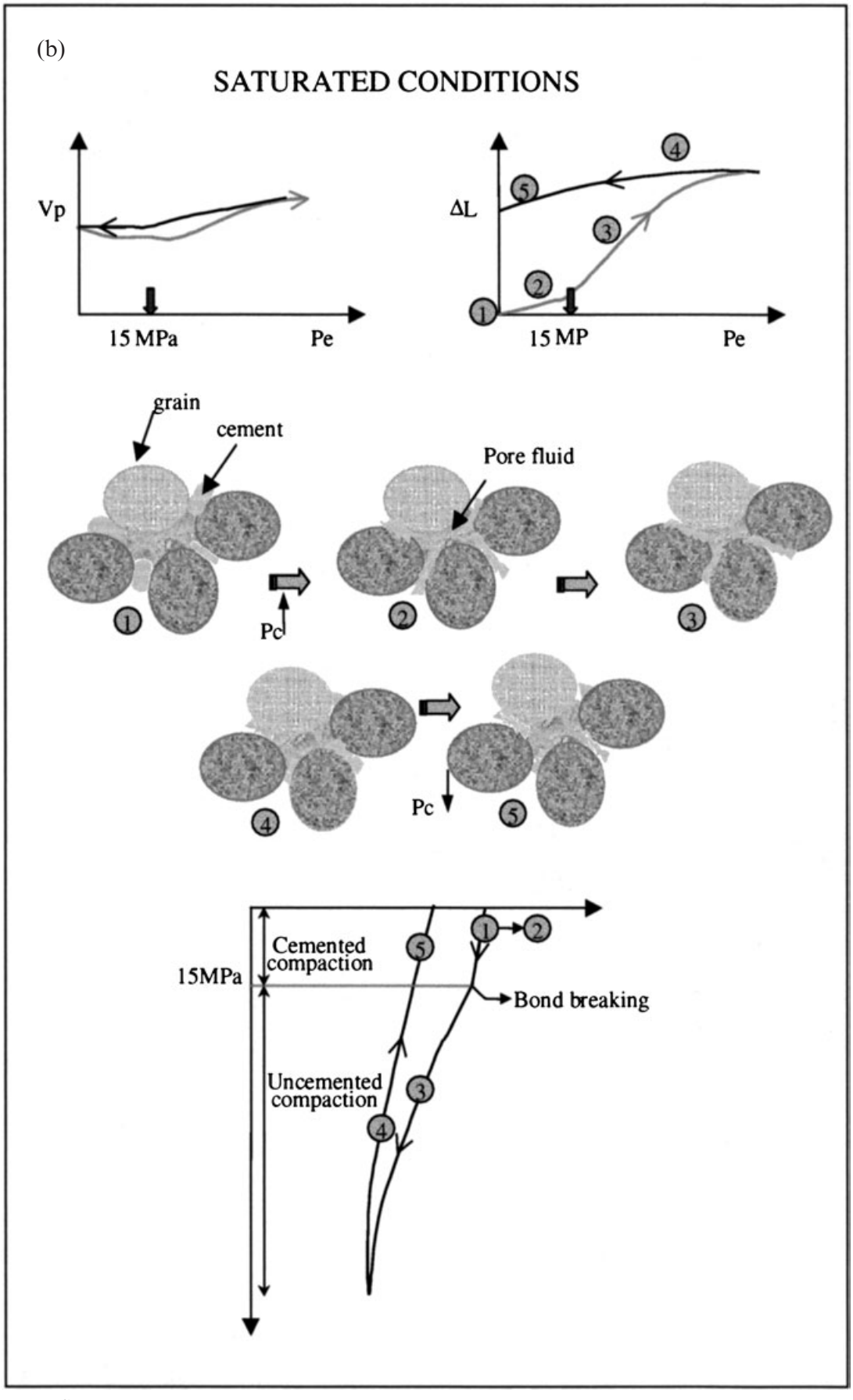

Figure 10. (*Continued.*)

pressure of the adsorbate (guest). It has been also demonstrated that the influence of the ion exchange can vary the adsorbate capacity; this effect, noted as the sentinel effect, is related to the change in internal zeolite size rings by the size of cations adsorbed (Rees 1984).

(4) Pressure and temperature significantly affect zeolite stability (Gillet *et al*. 1996; Boles *et al*. 1977). However, they are not considered significant for this study, because the measurements were conducted at pressures below those affecting zeolite stability and at room temperature conditions).

The pressure effects on physical and acoustic properties allow us to understand microstructural changes in these rocks. The changes in measured properties along with postulations about the main cause are schematized, for zeolitized pumice samples, in Fig. 10(a) for the dry and in Fig. 10(b) for the saturated case.

In dry conditions, the velocity decrease up to 15–20 MPa is due to breaking bonds around crystals and to the pumice collapse where the sample follows cemented compaction trend (Step 2 in Fig. 10a). After 15–20 MPa, compaction become significant as also testified by higher rate of DL change and the compaction follows the uncemented trend (Step 3 in Fig. 10a). The increasing pressure also breaks down the fibrous pumice structure (see Figs 6b and 9). For this reason, increasing pressure does not lead to a corresponding increase in velocity. When the pressure is released, the velocity values follow the uncemented compaction trend back (Step 4 in Fig. 10a). Especially below 15–20 MPa, since the broken bonds cannot be mended, a strong velocity decrease is observed (Step 5 in Fig. 10a). Porosity and permeability of the samples were measured after pressurization. An on average, the zeolitized pumiceous samples show 10 per cent change in porosity and more than 50 per cent in permeability. This is in contrast with no measurable change in the other samples and shows that in the former samples, pressure irreversibly reduces porosity and collapse of pumice will clog interconnected paths and lead to a permeability decrease.

Brine saturated samples (Fig. 10b) follow a similar path, a more marked velocity increase is noted due to high absorption power of zeolites (Step 3 in Fig. 10b). Upon pressure release, trapped pore waters due to pore collapse and to the aforementioned properties of zeolites lead to local pressure anomalies. The localized pore pressures changes might cause a stiffening of the frame, leading to increase V_p; V_s would not be affected (Step 4 in Fig. 10b). This hypothesis would also explain the different rates of DL change with pressure: the initial low rates are associated with the bond breaking and pumice collapse phase (Step 2 in Fig. 10b). Subsequent pressure increase leads to maximum compaction (Step 3 in Fig. 10b).

6 CONCLUSIONS

The main results of this study show that mineralogy and microstructure mainly affect the acoustic and petrophysical properties of these rocks under pressure condition. In particular:

(1) On the basis of rb-F relationship the analysed rock can be separated in three groups in according with their mineralogy.

(2) Zeolites and pumice significantly change the acoustic response in pyroclastic rocks (NYT and CIYF). Under the dry conditions, these changes are mainly due to the collapse of the internal texture of the pumice. In saturated conditions, additional effects are due to the water–zeolite interactions. CT-scans, optical microscopy, hydraulic and transport properties analyses supported changes in microstructure after pressure.

(3) Lava samples (ET and THR) show a slight velocity increases with pressure because of their stiffer frames and rounded pores (i.e. higher pore stiffness). Pyroclastic rocks whose velocity-pressure relationship is mainly controlled by microstructure, also show beyond 20 MPa a velocity increase with pressure associated with rounded pores rather than crack-closure.

We showed the importance of conducting velocity measurements at simulated *in situ* conditions both to estimate volcanic rock properties at depth and to identify relations between rock physics properties, confining and pore fluid pressure, and microstructure. Elastic parameters and rock physics relations at crustal condition are needed since they are involved into ground deformation model computations as well as control precursor phenomena in volcanic areas. Formulating reliable model permits a short-term prediction of a volcanic eruptive activity and therefore minimizes the hazard that it poses.

ACKNOWLEDGMENTS

We thank David A. DiCarlo for his help in making CT-scans, Giovanni Orsi and Raffaele Azzaro for their useful advice and help during the initial stages of this project. This work was supported by SRB Project and by the University 'Federico II' of Naples.

REFERENCES

Agip, 1987. *Geologia e Geofisica del sistema geotermico dei Campi Flegrei,* internal report., Milan, Italy.

Armienti, P., Barberi, F., Bizouard, H., Clochiatti, R., Innocenti, F., Metrich, N., Rosi, M. & Sbrana, A., 1983. The Phlegrean Fields: Magma evolution within a shallow chamber, *J. Volcanol. Geotherm. Res.,* **17,** 289–311.

Aster, R.C., Meyer, R.P., De Natale, G., Zollo, A., Martini, M., Del Pezzo, E., Scarpa, P. & Iannaccone, G., 1990. Seismic investigations of Campi Flegrei, Summary and Synthesis of the Results, in *Volcanic Seismology,* eds Gasparini, P., Scarpa, R., and Aky, K., pp. 462–483, Springer-Verlag, New York.

Birch, F., 1960. The velocity of compressional waves in rocks to 10 kilobars, Part 1, *J. Geophys. Res.,* **65,** 1083–1102.

Boles, J.R., Flanigen, E.M., Gude, A.J., Hay, R.L., Mumpton, F.A. & Surdam, R.C., 1977. Mineralogy and Geology of Natural Zeolites, ed Mumpton F. A., Mineralogical Society of America, Washington.

Bonafede, M., 1990. Axi-symmetric deformation of a thermo-poro-elastic half-space: inflation of a magma chamber, *Geophys J. Int.,* **103,** 289–299.

Breck, Donald, W., 1974. *Zeolite Molecular Sieves, Structure, Chemistry, and Use,* John Wiley and Sons, New York.

Carella, R. & Guglielminetti, M., 1983. Multiple reservoirs in the Mofete Field, Naples-Italy, *Proc. 9th Workshop Geothermal Reservoir Engineering,* pp. 28–32, Stanford University, Stanford.

Carmichael, R.S., 1989. *Practical Handbook of Physical Properties of Rocks and Minerals,* CRC Press, Boca Raton..

Casertano, L., Oliveri del Castillo, A. & Quagliariello, M., 1976. Hydrodynamics and geodynamics in Phlegraean Fields area of Italy. *Nature,* **264,** 5582–5586.

Cassano, E. & La Torre, P., 1986. Phlaegrean Fields area: geophysical contribution to geothermal prospecting, *Int. Symp Engineering Geol Problems in Seismic Areas, Geologia Applicata e Idrogeologia,* **4,** 39–56.

Civetta, L., Carluccio, E., Innocenti, F., Sbrana, A. & Taddeucci, G., 1991. Magma chamber evolution under the Phlegraean Fields during the last 10 ka: trace element and isotopic data, *Eur. J. Mineral.,* **3,** 415–428.

Civetta, L., Orsi, G., Pappalardo, L., Fisher, R.V., Heiken, G.H. & Ort, M., 1997. Geochemical zoning, mixing, eruptive dynamics and depositional processes—The Campanian Ignimbrite, Campi Flegrei, Italy, *J. Volcanol. Geotherm. Res.,* **75,** 183–219.

Di Maio, R. & Patella, D., 1994. Self-potential anomaly generation in volcanic areas: the Mt Etna case history, *Acta Vulcan.,* **4,** 119–124.

Dyer, A., 1988. *An Introduction to Zeolite Molecular Sieves,* John Wiley & Sons, New York.

Ferrucci, F., De Natale, G., Hirn, A., Mirabile, I. & Virieux, J., 1992. P-SV conversions at a shallow boundary beneath Campi Flegrei caldera (Naples, Italy): possible evidence for the magma chamber, *J. geophys. Res.,* **97,** 15 351–15 359.

Gillet, P., Maleziéux, J.M. & Itié, J.P., 1996. Phase change and amorphization of zeolites at high pressures: the case of scolecite and mesolite, *Am. Mineral.,* **81,** 651–657.

Hirn, A., Nercessian, A., Sapin, M., Ferrucci, F. & Wittlinger, G., 1991. Seismic heterogeneity of Mt Etna: structure and activity, *Geophys. J. Int.,* **105,** 139–153.

Lenzi, G. & Pozzuoli, A., 1970. Sul tufo zeolitizzato di Chiaiano (Napoli) e sulla determinazione del suo contenuto phillipsitico, Atti Accad, *Sci. Fis. Mat.,* **7,** 261–275.

Lirer, L., Luongo, G. & Scandone, R., 1987. On the volcanological evolution of Campi Flegrei, *EOS Trans Am. Geophys. Un,* **68,** 226–334.

Loddo, M., Patella, D., Quarto, R., Ruina, R., Tramacere, A. & Zito, G., 1989. Application of gravity and deep dipole geo-electrics in the volcanic area of Mt Etna (Sicily), *J. geophys. Res.,* **39,** 17–39.

Mauriello, P., Patella, D., Petrillo, Z. & Siniscalchi, A., 1997. Mount Etna structural exploration by magnetotellurics. *Acta Vulcanol.,* **9,** 141–146.

Orsi, G., De Vita, S. & Di Vito, M., 1996. The restless, resurgent Campi Flegrei nested caldera (Italy): constraints on its evolution and configuration, *J. Volcanol. Geotherm. Res.,* **74,** 179–214.

Prasad, M. & Manghnani, M.H., 1997. Effects of pore and differential pressures on compressional wave velocity and quality factor on Berea and Michigan sandstones, *Geophysics,* **62,** 1163–1176.

Prasad, M. & Nur, A., 2002. Relating texture and permeability anisotropy to velocity and attenuation anisotropy in sandstones, submitted.

Prasad, M., Palafox, G. & Nur, A., 1999. Velocity and Attenuation Characteristics of Daqing sandstones: Effects of permeability on velocity and attenuation anisotropy, AGU 1999 Fall Meeting, *EOS Trans. Am. Geophys. Un.,* **v,** 80.

Rees, L.V.C., 1984. Chemistry and Industry, ed. Derouane, E.G. *New York,* **7,** 253.

Rosi, M. & Sbrana, A., eds, 1987. Phlegraean Fields, *Quad, Ricerca Scientifica,* **114,** 1–175.

Rosi, M., Sbrana, A. & Principe, C., 1983. The Phlegraean Fields: Structural evolution, volcanic history and eruptive mechanism, *J. Volcanol. Geotherm. Res.,* **17,** 273–288.

Sersale, R., 1958. Genesi e costituzione del Tufo Giallo Napoletano, *Rend. Accad. Sci. Fis. Mat., Napoli,* **25,** 181–207.

Tanguy, J.C., Condomines, M. & Kieffer, G., 1997. Evolution of Mount Etna magma: constraints on the present feeding system and eruptive mechanism, *J. Volcanol. Geotherm. Res.,* **75,** 221–250.

Toksöz, M.N., Johnston, D.H. & Timur, A., 1979. Attenuation of seismic waves in dry and saturated rocks. I. Laboratory Measurements, *Geophysics,* **44,** 681–690.

Vanorio, T., 1998. Un modello 'elettrosismico' per la valutazione della porosità e del grado di saturazione di rocce, *Tesi di Dottorato in Geofisica e Vulcanologia—Università di Napoli 'Federico II',* University of Naples, Naples.

Zamora, M., Sartoris, G. & Chelini, W., 1994. Laboratory measurements of ultrasonic wave velocities in rocks from the Campi Flegrei volcanic system and their relation to other field data, *J. geophys. Res.,* **99,** 13 553–13 561.